Recent ASDEX Upgrade Research in Support of ITER and DEMO

H. Zohm for the ASDEX Upgrade Team and the EUROfusion MST1 Team[1]

Max-Planck-Institut für Plasmaphysik, Boltzmannstr. 2, D-85748 Garching, Germany

E-mail contact of main author: zohm@ipp.mpg.de

Abstract. Recent experiments on the ASDEX Upgrade tokamak aim at improving the physics base for ITER and DEMO to aid the machine design and prepare efficient operation. Type I Edge Localised Mode (ELM) mitigation using Resonant Magnetic Perturbations (RMPs) has been shown at low pedestal collisionality ($v^*_{ped} <$ 0.4). In contrast to the previous high v^* regime, suppression only occurs in a narrow RMP spectral window, indicating a resonant process, and a concomitant confinement drop is observed due to a reduction of pedestal top density and electron temperature. Strong evidence is found for the ion heat flux to be the decisive element for the L-H power threshold. A physics based scaling of the density at which the minimum P_{LH} occurs indicates that ITER could take advantage of it to initiate H-mode at lower density than that of the final Q=10 operational point. Core density fluctuation measurements resolved in radius and wave number show that an increase of R/L_{Te} introduced by off-axis Electron Cyclotron Resonance Heating (ECRH) mainly increases the large scale fluctuations. The radial variation of the fluctuation level is in agreement with simulations using the GENE code. Fast particles are shown to undergo classical slowing down in the absence of large scale MHD events and for low heating power, but show signs of anomalous radial redistribution at large heating power, consistent with a broadened off-axis Neutral Beam Current Drive (NBCD) current profile under these conditions. Neoclassical Tearing Mode (NTM) suppression experiments using Electron Cyclotron Current Drive (ECCD) with feedback controlled deposition have allowed to test several control strategies for ITER, including automated control of (3,2) and (2,1) NTMs during a single discharge. Disruption mitigation studies using Massive Gas Injection (MGI) can show an increased fuelling efficiency with High Field Side (HFS) injection, but a saturation of the fuelling efficiency is observed at high injected mass as needed for runaway electron suppression. Large locked

---

modes can significantly decrease the fuelling efficiency and increase the asymmetry of radiated power during MGI mitigation. Concerning power exhaust, the partially detached ITER divertor scenario has been demonstrated at P_{sep}/R = 10 MW/m in ASDEX Upgrade, with a peak time averaged target load around 5 MW/m^2, well consistent with the component limits for ITER. Developing this towards DEMO, full detachment was achieved at P_{sep}/R = 7 MW/m and stationary discharges with core radiation fraction of the order of DEMO requirements (70 % instead of the 30 % needed for ITER) were demonstrated. Finally, it remains difficult to establish the standard ITER Q=10 scenario at low $q_{95}=3$ in the all-tungsten (all-W) ASDEX Upgrade due to the observed poor confinement at low β_N. This is mainly due to a degraded pedestal performance and hence investigations at shifting the operational point to higher β_N by lowering the current have been started. At higher q_{95}, pedestal performance can be recovered by seeding N_2 as well as CD_4, which is interpreted as improved pedestal stability due to the decrease of bootstrap current with increasing Z_{eff}. Concerning advanced scenarios, the upgrade of ECRH power has allowed experiments with central ctr-ECCD to modify the q-profile in improved H-mode scenarios, showing an increase in confinement at still good MHD stability with flat elevated q-profiles at values between 1.5 and 2.

1. Introduction

ASDEX Upgrade is a medium-sized (R_0=1.65 m, a=0.5) tokamak with ITER-like coil and divertor geometry. Its main technical features include the three ITER day-1 heating systems, NBI (20 MW), ICRF (source power 8 MW) and ECRH (source power 6 MW, with 4.4 MW delivered to the plasma so far and an upgrade to 8 MW source power under way). The total installed source power of 34(36) MW together with the all-W wall makes ASDEX Upgrade ideally suited for studies of high performance plasmas and exhaust at high *P/R*. In addition, a set of 16 internal B_r coils, so-called B-coils, arranged in 2 rings above and below the outside mid-plane of the machine, can be used to generate *n=1, 2* and *4* resonant magnetic perturbations (RMPs). As of 2014, the phase of the B-coil currents can be slowly varied during the discharge. Also in 2014, ASDEX Upgrade was equipped with a new outer divertor

that features two rows of solid tungsten (W) tiles [1], replacing the W-coated C-tiles used elsewhere on the first wall to eliminate previous problems with delamination of W-coatings at high power. Also, a unique divertor manipulator was installed that allows insertion and removal of large area samples without machine opening [2]. In addition, two rows of bare P92 steel were installed at the inner heat shield [3]. Composition and ferro-magnetism of this material are close to the EUROFER steel envisaged as structural material in a European DEMO and are hence used to study the compatibility of a bare steel main chamber wall with high performance plasmas. The equilibrium reconstruction and control system had to be adapted to include the effect of the ferromagnetic components. Both extensions have performed very reliably throughout the whole campaign and did not lead to any restriction in operational space. Finally, the extensive set of high resolution diagnostics on ASDEX Upgrade is continuously extended. Two important examples from the 2013 and 2014 campaign are the dedicated fast ion diagnostics (Collective Thomson Scattering CTS, Fast Ion Loss Detectors FILD and Fast Ion D-Alpha spectroscopy FIDA) as well as the upgrade of microwave fluctuation diagnostics (see Section 3). Since 2014, a part of the ASDEX Upgrade programme is run in the framework of the MST campaigns of EUROfusion, emphasizing even stronger the collaborative nature of the programme. In 2014, about half of the experimental programme was carried out under EUROfusion.

Programmatically, research on ASDEX Upgrade aims at providing, in close collaboration with theory and modelling, the physics base for design and operation of ITER and DEMO. For the ITER Q=10 scenario, relatively low plasma performance ($H=1$, $\beta_N=1.8$ and $q_{95}=3$) is required. However, the need to limit the ELM size in this scenario calls for ELM control, e.g. by RMPs, which can impact the H-mode pedestal. In addition, past studies have shown that operation with the all-W covered wall of ASDEX Upgrade restricts the operational space to a region with potentially reduced pedestal performance. These findings have been confirmed

with the ITER-like wall on JET [4] and both machines explore ways to guarantee that ITER can reach its Q=10 goal. Concerning power exhaust, the figure of merit P_{sep}/R is of the order of 15 MW/m in ITER, assuming that it will be operated at $P_{sep} \approx 1.2 \times P_{LH}$. No experiment has yet demonstrated this power level at acceptable divertor heat flux $q_{div} \leq 10\ MW/m^2$ and it is one of the aims of ASDEX Upgrade to demonstrate a viable divertor solution for ITER employing conventional divertor geometry. For DEMO, the need to generate net electricity at reasonable recirculating power leads to an increase in the assumed values of β_N and H, requiring demonstration of a suitable operational scenario. It is hence another programmatic goal of ASDEX Upgrade to prepare such a scenario. The improved H-mode scenario is studied as a candidate, either in pulsed or in steady state mode, the latter depending on the achievement of sufficient bootstrap current fraction and efficient current drive schemes. The increased fusion power means that in DEMO, P/R will be largely increased w.r.t. ITER: if the ITER divertor solution at P_{sep}/R = 15 MW/m together with $P_{sep} \approx 1.2 \times P_{LH}$ is assumed, the fraction of radiated power from the core will have to be increased substantially, to $P_{rad,core}/P_{tot}$ 1 - P_{sep}/P_{tot} = 0.7 - 0.8, as opposed to 0.3 in ITER. It will also be beneficial to operate DEMO at higher n/n_{GW} than ITER [5]. Finally, disruptions pose a serious problem for both ITER and DEMO and efficient mitigation schemes need to be developed.

This paper is hence organized as follows: in sections 2 to 6, recent results concerning the individual physics elements needed to fulfill the requirements outlined above are discussed. In Section 7, we discuss the challenges arising from putting together these elements into a consistent operational scenario, both in terms of core confinement as well as taking into account the restrictions arising from the exhaust scheme.

2. Application of 3-D fields for ELM control

The application of 3-D fields is tightly linked to the question of error field penetration. In ohmic L-mode plasmas at low rotation and low density, during application of RMPs a change in the E_r well structure is found, with E_r changing sign in some region close to the separatrix. This is interpreted as an indication of stochastisation and hence parallel losses dominating the sign of E_r [6]. Under these conditions, i.e. low rotation and density, the penetration of RMP generated error fields follows the picture outlined in [7]: for a slow ramp in RMP current, no penetration is observed until at a critical value, plasma rotation stops and a large island occurs. This island is shifted in phase, which is partly attributed to the remaining torque leading to 'natural' rotation when there is no mode. However, in experiments with NBI where a pre-existing tearing mode locks to the RMP field, there is evidence that the torque is not only a local $j{\times}B$ torque at the dominant resonant surface, but also affects other surfaces [8], indicating that the response of several surfaces has to be taken into account to correctly describe the mode penetration, consistent with RMP penetration experiments in other devices [9]. In high collisionality strongly rotating H-modes, the plasma core is hardly affected by RMPs, consistent with a strong shielding and a negligible contribution of Neoclassical Toroidal Viscosity (NTV) [8]. Contrary, at low collisionality, a density decrease is observed as well as an effect on the rotation profile, indicating a plasma response.

Previous experiments on ELM mitigation in the high collisionality regime have shown a wide window of q_{95} and RMP spectrum to be effective, i.e. with no clear indication for a resonant process [10]. This is different from recent experiments that show ELM mitigation at low collisionality ($v^*_{ped} < 0.4$). An example for stationary ELM mitigation at optimum phase angle $\Delta\Phi=90°$ is shown in Fig. 1. A slow phase scan between the currents in the upper and the lower RMP ring, both operated in n=2 configuration, shows the existence of RMP spectral

windows in which ELMs can be strongly mitigated [11]. These windows do not exactly coincide with resonant alignment of the vacuum field with the unperturbed plasma field, indicating a response of the plasma that modifies the spectral content. Specifically, in the edge region of these discharges, low-n peeling modes seem to be dominant in amplifying the RMP field [12].

It can be seen that there are still ELM-like events, albeit at much reduced amplitude and strongly increased frequency, reminiscent of the low-collisionality ELM mitigation regime in KSTAR [13] and probably different from the DIII-D results which show complete suppression in this collisionality regime [14]. We note however, that below a certain threshold, also on DIII-D, mitigation rather than suppression is observed and it can at present not be ruled out that such a threshold exists in ASDEX Upgrade as well, but has not yet been reached. As in other devices, in this regime, a clear degradation of pedestal parameters is observed, leading to a reduction of confinement in the regime with clear ELM mitigation. This is partly due to the above mentioned decrease of density, which affects the whole profile and hence also the pedestal top value, but, as can be seen in FIG.1, also a decrease of the pedestal ion temperature, while the electron temperature remains unaffected.

3. L-H transition and pedestal physics

Recent work on the L-H transition was focused on the identification of the physical parameters determining the power threshold. Previous work on the low density branch of the P_{LH} threshold [15] had already indicated that the decoupling of ion and electron channel is responsible for the observed increase of P_{LH} when applying ECRH at low density. Recent transport analyses in the low density branch, [16], reveal that the edge ion heat flux at the LH transition ($Q_{i,edge}$) increases linearly with density, despite the non-monotonic behavior of P_{LH} ,

FIG. 2 left panel. This is consistent with the fact that the edge E_r shear, assumed to be the cause of the LH transition, is essentially induced by the main ion pressure gradient in ASDEX Upgrade [17], as predicted by neoclassical theory.

This is also consistent with our previous finding that the L-H transition occurs at a critical value of minimum E_r , [15], since the width of the E_r well is found to not vary strongly in ASDEX Upgrade [17]. Furthermore, as shown in FIG. 2, $Q_{i,edge}$ is independent of plasma current, in contrast to P_{LH} in this lower density range. This is due to the I_p dependence of confinement. Based on confinement and energy exchange considerations (as expressed by the ratio τ_{ei}/τ_E), in which the machine size plays a key role, a scaling for the density at which P_{LH} has its minimum can be derived by fitting data from different tokamaks in the ITPA database: $n_{e,min}{}^{scal} = 0.7\ I_p{}^{0.34}\ a^{-0.95}\ B_t{}^{0.62}\ (R/a)^{0.4}$.   This scaling consistently orders the experimental data from the various devices, as shown in the right part of FIG.2, albeit some of the variations observed in individual machines cannot be described consistently. It predicts 4×10^{19} m^{-3} for the ITER Q=10 scenario (2.2×10^{19} m^{-3} at half field and current), which means that the Q=10 operation point is in the regime where the usual linear scaling applies, and inducing the L-H transition at lower density at a time when the fusion power is not yet fully developed will also lower the threshold power down to the values quoted above. Generally, the global P_{LH} in the intermediate density range is lower by about 25 % in the all-W ASDEX Upgrade as compared to the C wall, [18]. This behavior, also seen in JET with the ITER-like wall (ILW) [19], may be due to a steepening of the edge density profiles in L-mode with the W-wall.

On the high density branch, it is well known that there is an upper density limit to H-mode operation. On ASDEX Upgrade, it is found that this limit consists of 4 distinct phases that can be universally characterized in a diagram of edge density and temperature [20]. Increasing the density, there first is a regime where $n_{e,lin}$ can be increased by gas puff and the pedestal top

density and temperature roughly follow an isobar. This is followed by a regime where $n_{e,lin}$ saturates while the Scrape-Off Layer (SOL) density still increases and confinement starts to degrade due to a decrease in pedestal temperature, with the pedestal top pressure deviating from the above mentioned isobar. In the third phase, the pedestal temperature severely erodes, leading to a decrease of the depth of the E_r well until finally, the H-L transition occurs, with the back transition taking place at roughly the same depth of the E_r well that is needed to transit into H-mode, indicative of the mean shear flow being responsible for both L-H and H-L transition. The pedestal degradation comes together with a change in SOL turbulence characteristics, mainly a strong increase in filamentary transport [21] suggesting that also transport inside the separatrix could be increased. This increase, which has also been found in L-mode [22] is especially pronounced once the outer divertor detaches, which has been linked to the different boundary condition for filament currents when the electrical connection to the plate is lost. In the following L-mode phase, $n_{e,lin}$ can again be increased until a disruptive density limit following the occurrence of a MARFE occurs. Hence, the H-mode density limit can be viewed as an edge density limit, not principally limiting the central density that can be achieved in H-mode. This has been demonstrated using pellet fuelling where H-modes have been achieved up to line averaged densities of $n/n_{GW} = 1.5$ due to profile peaking, but the pedestal top density stayed below $n/n_{GW} = 1$ [23]. While pellets are an efficient tool to peak the density in ASDEX Upgrade, pellet penetration is expected to be too shallow in DEMO for this effect. On the other hand, theory predicts a substantial peaking of the DEMO density profile due to the turbulent inward pinch occurring at low collisionality which indicates that DEMO could run at line averaged densities above n_{GW} [5].

It was shown before on ASDEX Upgrade and JET that operation with a metal wall pushes the operational window to higher gas puff and density, accompanied by a loss of pedestal pressure. This can be recovered by N_2 seeding. More recent studies show that this result can

also be obtained in the all-W ASDEX Upgrade by CD_4 seeding. With both seed gases, the pedestal top temperature can be improved, at constant input power, by up to 40% w.r.t. the degraded situation, leading to an overall increase of the stored energy of roughly that value due to the stiff temperature profiles (R/L_T hardly changes). Detailed analysis of the edge profiles shows that the peak of bootstrap current density, which experimentally has been found to be consistent with the value calculated using the Sauter formula [24], is lower with N_2-seeding due to the higher Z_{eff}, which increases the margin until the linear peeling-ballooning stability is hit [25]. The effect of N_2-seeding is similar at low ($\delta \approx 0.25$) and higher ($\delta \approx 0.35$) triangularity, with high triangularity itself adding another 10-20% of pedestal top pressure. Concerning ELM losses, the nonlinear ELM phase characterized by strong filamentary losses can have a much longer duration in the all-W ASDEX Upgrade and also in JET with the ILW than observed with carbon (C)-wall. N_2- and CD_4-seeding show a tendency to reduce the ELM duration, leading to smaller ELM-losses [26]. Clearly, this phenomenon cannot be described by linear physics since the onset of both long and short ELMs is similar, and it seems that the duration of the nonlinear phase is rather correlated to the SOL/divertor temperature which will change, e.g., the SOL collisionality. In general, while linear peeling-ballooning analysis often describes reasonably well the type I ELM onset in ASDEX Upgrade, there are also cases in which clear discrepancies exist, indicating the need for additional physics elements to obtain a predictive capability for the H-mode pedestal [27].

4. Core confinement

One of the aims of recent studies of core transport has been to address in-depth validation of turbulence codes on a microscopic level by experimental studies of turbulence characteristics. Within this initiative, the so-called 'HGF Virtual Institute for Advanced Microwave

Diagnostics', a first step has been to obtain radially resolved density fluctuation levels by Doppler reflectometry, which can also distinguish different $k_\perp$-ranges. Here, $k_\perp$ is the wavevector perpendicular to B and tangential to the flux surface. In a series of H-mode discharges, ECRH deposited at half radius was used to vary R/L_{Te}, which is one of the drivers of turbulence. The pronounced changes in this parameter also lead to changes in R/L_n and R/L_{Ti}, providing a strong variation in the source term for turbulence [28].

As can be seen from FIG.3, under these conditions, the radial profiles of density fluctuation amplitude show the well-known increase with radius up to the E_r shear region. Concerning the wavenumber dependence, a pronounced increase of large scale (i.e. $k_\perp$ in the range of 4-8 cm^{-1}) turbulence is detected when ECRH is used to increase R/L_{Te}. In the higher $k_\perp$-ranges accessible to the experiment (8-13 cm^{-1} and 13-18 cm^{-1}), such an increase is not observed. It can also be seen that the absolute level is lower at higher wavenumber, consistent with the usual decay of spectral power as function of $k_\perp$. Comparing these findings to local nonlinear flux-matched turbulence simulations using the GENE code [29], it is found for all points shown in Fig. 3 that the dominant unstable mode propagates in ion-diamagnetic direction, which corresponds for these scales to the ITG instability in the GENE code. It can also be seen in FIG.3 that GENE reproduces the radial variation of the turbulence level for moderate ECRH power, albeit at present, it cannot reproduce the increase in fluctuation amplitude at low $k_\perp$ during ECRH. Understanding the increase in large scale fluctuations, however, is still ongoing. Future work will also include T_e fluctuation measurements and hence address the cross-phase between n_e and T_e fluctuations, which will provide a stringent test of the theoretical modelling.

Another important aspect is the confinement and slowing down of fast particles since it determines the heating profile and efficiency in future reactor grade plasmas as well as the

efficiency of NBCD in present and future experiments. The set of fast particle diagnostics on ASDEX Upgrade has been continuously increased, now consisting of CTS, two FIDA systems with poloidal and toroidal sightlines and two FILDs. Studies of the NBI created fast ion slowing down [30] revealed that for large MHD events such as sawteeth, radial transport is clearly anomalous, while in the absence of large scale MHD modes and Alfvén Eigenmode activity, it is mainly consistent with the neoclassical prediction. The redistribution of fast ions during sawtooth crashes was found to be consistent with a simple Kadomtsev reconnection model assuming that the fast ions are convected with the field lines during reconnection. Previous studies of the radial fast ion profiles during off-axis NBCD at medium power (5 MW) revealed neoclassical behavior, while more recent studies at higher heating power (10 MW) show signs of a discrepancy. This is consistent with earlier findings that at high heating power, the profile of driven current is different from the neoclassical prediction while the value of the total driven current is roughly in line with the neoclassical prediction. FIG.4 shows a comparison between experimental results and theoretical modelling. The left part shows a discrepancy between the neoclassical prediction and the measured FIDA signals in the region of interest for off-axis NBCD in these experiments, i.e. roughly between $\rho=0.3$ and $\rho=0.5$, and the lower signal amplitude can be reproduced assuming a moderate anomalous transport level of ~ 0.5 m^2/s, which could be due to the effect of turbulent transport on the fast particles. On the right side of FIG.4, it can be seen that this level of anomalous fast particle transport also best matches the measured temporal evolution of the MSE measurement.

Finally, recent experiments on fast particle driven modes indicate that at the highest beam energy (93 keV) in ASDEX Upgrade, the modes can already have a bursting character indicating nonlinear interaction between individual modes rather than just a 'sea of Alfven modes' that individually contribute to transport of fast ions.

5. MHD modes and disruptions

In this area, a focus was laid on the feedback controlled suppression of NTMs by ECCD [31]. A versatile NTM control system was implemented in the framework of the ASDEX Upgrade discharge control system (DCS) [32]. The NTM amplitude and mode number are determined in real time from a combination of Mirnov coils. The resonant surface can be determined either from cross correlation of Mirnov coils and Electron Cyclotron Emission (ECE) or from equilibrium reconstruction, the latter with the advantage that it also works when no mode is present, i.e. in pre-emptive operation. By optimizing the parameters of the equilibrium reconstruction, that is at present obtained from magnetic measurements alone, the error in determination of the resonant surface has been reduced to $\Delta\rho \leq 0.05$, sufficient for suppression of large NTMs, and this scheme is usually applied. Combining equilibrium reconstruction and online density measurements [33], TORBEAM [34] analysis is done to obtain the ECCD deposition and DCS then acts to overly ρ_s and ρ_{dep} by moving the ECCD launching mirror, which is the actuator also foreseen for application in ITER.

This flexible implementation opens the possibility of testing different control strategies to find the optimum solution for ITER. So far, different strategies for deposition control were tested, including sweeping across the resonant surface to find the minimum in mode amplitude, feedback based on temporal evolution of the mode amplitude for small steps and feedforward oscillation around the ρ_{NTM} value determined in real time. The latter is favorable if the uncertainty in ρ_{NTM} is larger than the deposition width and leads to complete suppression if the power level is sufficient. Future strategies will include systematic study of the already implemented feedback of ECCD power and use of a FADIS inline-ECE system for detecting the resonant surface as well as use of equilibrium information from online prediction of the discharge evolution using the RAPTOR code [35]. The present control can

also target more than one surface, and an example of a discharge where the DCS automatically changes the target is shown in FIG.5. Here, an initial (3,2) NTM is fully suppressed by targeting the q=1.5 surface (black crosses in Fig. 5 b), from ECE/Mirnov analysis, $\rho_{(m,n)}$ from equilibrium reconstruction shown for information only). Later in the discharge, a (2,1) NTM occurs and DCS recognizes from the mode amplitudes shown in FIG. 5 c) that this is the dominant mode, changes the target to the q=2 surface, and suppresses the mode there.

In ITER and DEMO, disruptive termination of a full performance discharge will pose a serious threat to the device integrity due to the high thermal and mechanical loads associated with these events. While the NTM stabilization schemes outlined above aim at controlling MHD instabilities that may lead to a disruption, we also study the mitigation of the consequences of disruptions. Mitigation studies using a Massive Gas Injection (MGI) of Ne have been conducted with valves located close to the plasma, both on the Low Field Side (LFS) and High Field Side (HFS) [36]. In the parameter range suitable for mitigation of the Thermal or Current Quench (TQ or CQ), HFS MGI has a significantly higher fuelling efficiency than LFS injection. However, when further increasing the amount of injected gas to reach a density in the range of that needed for collisional runaway electron suppression, both LFS and HFS schemes show a dramatic decrease of the fuelling efficiency and hence a saturation of the total electron density at values around 25 % of the predicted critical ('Rosenbluth') density. The fuelling efficiency hardly depends on the plasma thermal energy. However, it was found that injection into pre-existing locked modes, which might well occur in ITER shutdown scenarios, decreases the number of impurity atoms assimilated by the plasma before the TQ by shortening the time interval between arrival of the gas and occurrence of the TQ [37]. Finally, locked modes can also enhance the asymmetry of the energy radiated to the wall in the pre-TQ phase. We also note that stable long-lived (up to 200

ms) runaway electron discharges have been obtained by triggering the CQ in very low density plasmas using high pressure impurity injection; these can serve as target for runaway electron dynamics studies in future.

6. Exhaust physics

Recent work analyzing the scaling of λ_q, the SOL power decay length in the outside midplane has revealed a clear $1/B_p$ dependence with no size scaling [38], leading to the prediction of a very narrow power decay length in ITER and DEMO and emphasizing the importance of the figure of merit for exhaust, P_{sep}/R, since as a consequence of this scaling, the wetted area for power will only increase linearly in R. In order to determine the heat flux profile on the divertor plates, it is important to also understand the broadening of the heat flux profile by geometrical effects (flux expansion f_x) as well as perpendicular transport. The latter has been parametrised by the power spreading factor S that is obtained assuming a Gaussian spreading of profile in the perpendicular direction due to diffusion so that λ_{int}, the profile width on the target plate is to a good approximation given by $f_x\,\lambda_{int} = f_x\,(\lambda_q + 1.64\,S)$. Recent studies on ASDEX Upgrade and JET have focused on the scaling of S with plasma parameters [39]. In attached ELMy H-mode cases, it is found that, similar to λ_q, S scales close to linear with $1/B_p$, but this quantity also exhibits a strong size scaling of $R^{0.7}$. The latter is interpreted as an effect of the connection length, since for constant ratio of perpendicular to parallel transport, the broadening should increase with the connection length. Relating S to divertor parameters shows a strong correlation with $1/T_{div}$, the electron temperature at the target plate. This is again in line with diffusive broadening since parallel transport will decrease strongly with decreasing T_{div}. These effects have also been verified using the SOLPS code [40]. However, inserting the numbers, even at very low T_{div} around 5 eV, the maximum heat load in a DEMO

would exceed the component limit [39]. We remind here, though, that the scalings discussed above hold under attached conditions, and hence, as is done for ITER, detached operation should be envisaged for DEMO and the power loads should be characterized under these conditions.

Experimentally, partial detachment of the divertor, i.e. a strong decrease of the pressure along field lines close to the separatrix where the SOL flux tubes are longest, drastically reduces the peak heat flux and may be sufficient for ITER. On the other hand, for DEMO, it has been shown that full detachment will be required due to the energy form recombination at the target that represents an irreducible offset for the power flux to the plate in the attached region [41]. Recent experiments employing Nitrogen as divertor radiator have succeeded in partial detachment at values up to $P_{sep}/R = 10$ MW/m, with time averaged peak target load of around 5 MW/m^2, i.e. well within the ITER requirements [42]. These conditions are achieved in stable H-mode conditions by feedback controlling the N$_2$-flux to obtain a preset divertor temperature represented by a thermo current into the outer divertor plate [43]. At lower power levels, $P_{sep}/R \leq 7$ MW/m, full detachment can be obtained using N$_2$-seeding and heavy D$_2$-puffing [44], leading to a strong reduction in the flux to the target with the target power load dropping below the detection limit. This is usually accompanied by strong X-point radiation and a rise in the pedestal and line-averaged density, which is thought to be due to improved fuelling since the high density structures in the divertor observed with partial detachment [45] are no longer present with full detachment. Concomitantly, a modest (10-15%) drop of stored energy at total heating power, i.e. a degradation of global energy confinement, is observed. Future work will aim at controlling these operational issues linked to full detachment.

Modelling detachment with the SOLPS code shows good agreement for attached L-mode cases when the drifts are fully included [46], although the modelled target flux in the rollover regime is still significantly lower than the experimentally measured one. The inner divertor,

in contrast, is not well described, although the inclusion of drifts improves somewhat the results. Furthermore, it is now possible to obtain detached solutions for the outer divertor under H-mode conditions, with outer target profiles well matching the experiment [47].

7. Scenario Integration

In this section, we treat the integration of the different physics elements discussed before into an operational scenario. It is important to note that the operational range of present day experiments can usually match well the dimensionless parameter β envisaged for ITER and DEMO, while the normalized Larmor radius ρ^* cannot be met. In addition, it is either possible to match the normalized collisionality ν^* or the density normalized to the empirical Greenwald limit, $f_{GW}=n/n_{GW}$, but not both simultaneously. While one can argue that for core physics, ν^* is probably the more important of the two, edge, SOL and divertor physics also shows a strong variation with f_{GW}. In fact, due to the importance of atomic physics in the SOL and divertor radiation, it is more important to match the absolute values of density and temperature there. Due to the aforementioned preference to operate the all-W ASDEX Upgrade at high density, our studies usually focus on this parameter range. Together with the large P_{sep}/R, and the similarity of the predicted λ_q between ASDEX Upgrade, ITER and DEMO, it can actually be argued that the divertor conditions in ASDEX Upgrade are quite similar to those expected in ITER and DEMO. Finally, we mention here that high power scenarios in ASDEX Upgrade usually apply dominant unidirectional NBI heating leading to core Mach numbers substantially higher than those expected in ITER and DEMO. Since it is expected that the Mach number can have an influence on both confinement and stability, this has to be taken into account when extrapolating a scenario to these devices. In future, the

increased RF power in ASDEX Upgrade can be used to experimentally vary the Mach number profile at constant heating power, allowing to some extent to study these issues.

7.1 ITER Q=10 Scenario ('Baseline')

Studies to establish operation fulfilling the requirements of the ITER baseline scenario in the all-W ASDEX Upgrade have progressed to obtain long stationary discharges at the ITER values of δ, q_{95}, β_N and f_{GW}, so that, as pointed out above, ν^* is not matched, by applying X3 ECRH or Ion Cyclotron Resonance Heating (ICRH) at 1.8 T ($I_p = 1.1$ MA) and 2 T ($I_p = 1.2$ MA) to provide the central heating needed to avoid W accumulation.

As can be seen in the left panel of FIG. 6, the necessary values of $H=1$ and $n/n_{GW}=0.85$ can be reached with both W- and C-wall, but from the right panel of FIG. 6, it becomes clear that at the ITER baseline β_N value of 1.8, confinement is usually below the ITER Q=10 goal with W-wall while with C-wall it had been reached. This is attributed to the above mentioned degradation of the H-mode pedestal in the all-W device and is also found at JET with the ILW [48]. First attempts to recover confinement by N_2-seeding, as described in Section 3 for higher β_N cases, resulted in a decrease of ELM frequency, probably due to the reduced P_{sep}, and concomitant impurity accumulation in these cases. Another challenge is that in this corner of parameter space, ELMs are large and the mitigation methods established on ASDEX Upgrade (RMPs in the high density branch and pellet pacing) have not shown success so far. Pellet pacing in these discharges faces an 'inhibit' time after an ELM event during which no ELM can be triggered, limiting the maximum pacing frequency. With the C-wall, this had not been observed, and the difference seems to be due to a different build-up of the pedestal pressure after the long lasting ELMs observed with the W-wall at low heating power (see also Section 3).

A possible strategy to overcome some of these shortcomings aims at operation at higher β_N, since, as also found on other devices, H is usually higher in the operational range with higher β_N in ASDEX Upgrade (see also right panel of FIG. 6). Since, at constant heating power, the fusion power sales like $Q \sim H\beta_N/q_{95}^2$, an operational point with lower current can give the same Q if H increases strongly enough. Operating at higher q_{95} has some other benefits, such as the existence of RMP ELM mitigation schemes and a lower disruptivity. Experiments have hence been carried out that demonstrate that the same stored energy can be achieved with same toroidal field, heating power and line averaged density, but reduced plasma current [49]. FIG. 7 shows an example with a 20 % reduction of I_p. One element in this scenario is that at higher q_{95}, the plasma is less prone to impurity accumulation and hence the gas puff can be reduced. We note that both discharges have the same n/n_{GW}, which means lower absolute density for the higher q_{95} case, but the relatively small difference should not change the fusion power as long as the operational point is around the optimum temperature where $P_{fus} \sim (nT)^2$. On the other hand, the lower absolute value of density could be problematic for the exhaust scenario and hence we will also study to what extent line averaged density and separatrix density can be varied independently, e.g. by a combination of pellet fuelling and gas puff. However, it can be seen in FIG. 7 that the ELM frequency is still low in the $q_{95}=3.6$ case and RMP suppression of ELMs has not been successful so far. Also, it is important to point out that for the comparison shown in FIG. 7 the values of $H = 0.9$ for the baseline case at $q_{95}=3$ and $H=1.1$ for the reduced current at $q_{95}=3.6$, i.e. are below the ITER performance target. Evaluating $H\beta_N/q_{95}^2$, we find it is still about 10 % short of the value needed for Q=10. Hence, further studies will target at improving the confinement at higher q_{95} along the lines outlined in section 3, i.e. use N_2-seeding to recover pedestal performance to understand if this scenario can be considered as a candidate for an 'alternative Q=10 baseline scenario' for ITER.

7.2 Scenarios with performance above the ITER baseline

The alternative baseline scenario described above is of the 'improved H-mode' type studied previously on ASDEX Upgrade and also on DIII-D, where it is dubbed 'advanced inductive' scenario and on JET and previously on JT-60U (known as 'high β_N-scenario' there). This scenario usually avoids sawteeth by keeping q_0 just above 1 and values of $1.2 \leq H \leq 1.5$ can be achieved at β_N values up to 3, limited by the occurrence of NTMs [50]. The question arises if it is possible to raise q_0 in this scenario to avoid the $q=1.5$ and even the $q=2$ surface and hence the NTMs of that mode number. In addition, this will raise, for given β_N, the bootstrap fraction, thus increasing pulse length or even allowing steady state operation in DEMO with acceptable auxiliary current drive [51]. Experiments using central counter-ECCD as a tool to modify the q-profile in this direction became possible in 2014 due to the increased ECCD power. First experiments show that q in the flat central region can be raised significantly, to values between 1.5 and 2 according to MSE measurements if the central counter-ECCD is well positioned [52]. So far, at q_{95} around 5 and in the range $2 < \beta_N < 2.5$, confinement improves significantly, from $H=0.9$ in the standard H-mode up to $1.3 < H < 1.5$. An NBI power ramp indicates a β-limit of $\beta_N=3.8$, due to a (2,1) NTM, so there is still headroom to further optimize this scenario with even more ECCD power becoming available in the future.

7.3 Consistent Exhaust Scenarios for DEMO

As shown in Section 6, stationary exhaust at steady-state exhaust compatible target load has been demonstrated with N_2-seeding and strong D-puff leading to a partially detached divertor up to $P_{sep}/R = 10$ MW/m, corresponding to 2/3 of the value required for ITER and DEMO. It was mentioned in Section 1 that for DEMO, a higher core radiated fraction is needed if the ITER divertor solution is to be adopted. Studies of this scenario have been performed in ASDEX Upgrade using simultaneous feedback controlled injection of N_2 to cool the divertor

and Ar or Kr to increase the core radiation. Fig. 8 shows the operational space of ASDEX Upgrade employing up to 26 MW of heating power [42].

It can be seen that DEMO relevant core radiation fractions have been obtained, albeit at relatively low P_{sep}/R while on the other hand, the data points approaching the ITER and DEMO relevant P_{sep}/R are at the lowest core radiation fraction. As can also be seen from the diagram, further extension needs an increase of the total applied heating power above the present maximum value of 26 MW. The present limitation to this value is partly due to technical reasons connected to limitations of the heating systems and the power supplies. An extension is under way that should allow injecting simultaneously 34 MW in 2018, which would allow the demonstration of the necessary P_{sep}/R values for ITER and DEMO. It is also clear that even this value will not allow a simultaneous demonstration of core radiation fraction and power across the separatrix needed for DEMO.

Another limitation to the applicable heating power is the β-limit. Since, as discussed above, both N$_2$-seeding and operation at high β_N have a tendency to increase confinement, many of the operational points shown in FIG. 8 actually have H-factors 1-1.2, even for the highest core radiation fraction and without correcting for core radiation in the determination of H, and β_N-values around 3, limited by the occurrence of NTMs. While this is in itself a proof that attractive operational scenarios should exist in this corner of operational space for DEMO, it will require simultaneous development of adequate core scenarios including active NTM control at high density to be able to inject the above mentioned 34 MW into relevant high performance plasmas.

8. References

[1]   A. Herrmann et al., "Solid tungsten Divertor-III for ASDEX Upgrade and contributions to ITER", paper presented at 25th IAEA Int. Conf. on Fusion Energy St. Petersburg (2014).

[2]   A. Herrmann et al., 28th SOFT conference (2014), to appear in Fus Eng. Design.

[3]   I. Zammuto et al., 28th SOFT conference (2014), to appear in Fus. Eng. Design.

[4]   F. Romanelli et al., "Overview of the JET results", paper presented at 25th IAEA Int. Conf. on Fusion Energy St. Petersburg (2014) OV/1-3.

[5]   H. Zohm et al., Nucl. Fusion **53** (2013) 073019.

[6]   G. Conway et al., to appear in Plasma Phys. Control. Fusion (2014).

[7]   R. Fitzpatrick, Nucl. Fusion **33** (1993) 1049.

[8]   S. Fietz et al., Nuclear Fusion **55** (2015) 013018.

[9]   J.-K. Park et al., Phys. Rev. Lett. **99** (2007) 195003.

[10]   W. Suttrop et al., PRL **106** (2011) 225004.

[11]   W. Suttrop et al., "Studies of magnetic perturbations in high-confinement mode plasmas in ASDEX Upgrade", paper presented at 25th IAEA Int. Conf. on Fusion Energy St. Petersburg (2014) EX/P1-23.

[12]   D.A. Ryan et al., Joint EU-US Transport Task Force Workshop (2014) Culham, U.K.

[13]   J. Kim et al, Nucl. Fusion **52** (2012) 114011.

[14]   T. Evans et al., Nucl. Fusion **48** (2008) 024002.

[15]   P. Sauter et al., Nucl. Fusion **52**, (2012), 012001.

[16]   F. Ryter et al., Nucl. Fusion **54** (2014) 083003.

[17]   E. Viezzer et al., Nucl. Fusion **53** (2013) 053005

[18]   F. Ryter et al., Nucl. Fusion **53** (2013) 113003.

[19]   C.F. Maggi et al., Nucl. Fusion **54** (2014) 023007.

[20]   M. Bernert et al., Plasma Phys. Control. Fusion **57** (2015) 014038.

[21]   H.-W. Müller et al., 21st PSI conference, submitted to Journal Nucl. Materials (2014).

[22]   D. Carralero in , Nucl. Fusion **54** (2014), 123005.

[23]   P.T. Lang et al., Nucl. Fusion **52** (2012) 023017.

[24]   M.G. Dunne et al., Nucl. Fusion **52** (2012) 123014.

[25]   M.G. Dunne et al., 41st EPS conference on Plasma Physics (2014) P2.071.

[26]   P. Schneider et al., Plasma Physics and Controlled Fusion **56** (2014) 25011.

[27]   E. Wolfrum et al., "Overview of recent pedestal studies at ASDEX Upgrade", paper presented at 25th IAEA Int. Conf. on Fusion Energy St. Petersburg (2014) EX/3-1.

[28]   T. Happel et al., "Core turbulence behaviour moving from ITG towards TEM regime in the ASDEX Upgrade tokamak and comparison with gyrokinetic simulation", submitted to Phys. Plasmas (2015).

[29]   F. Jenko et al., Phys. Plasmas **7** (2000) 1904-1910.

[30]   B. Geiger et al., Plasma Phys. Control. Fusion **57** (2015) 014018.

[31]   M. Reich et al., "Real-time control of NTMs using ECCD at ASDEX Upgrade", paper presented at 25th IAEA Int. Conf. on Fusion Energy St. Petersburg (2014) PPC/P1-26.

[32]   W. Treutterer et al., Fusion Engineering and Design **89** (2014) 146.

[33]   A. Mlynek et al., Nucl. Fusion **51** (2011) 043002.

[34]   E. Poli et al., Comp. Phys. Comm. **136** (2001) 90.

[35]   F. Felici et al., Nucl. Fusion, **51** (2011) 083052.

[36]   G. Pautasso et al., submitted to Nucl. Fusion (2014).

[37]   G. Pautasso et al., 40th EPS Conference on Plasma Physics (2013) O5.104.

[38]   T. Eich et al., Phys. Rev. Lett **107** (2011) 215001.

[39]   B. Sieglin et al., PhD thesis, Technical University of Munich (2014).

[40]   A. Scarabosio et al., 21st PSI Conference, submitted to Journal Nucl. Materials (2014).

[41]   A. Loarte et al., Progress in the ITER Physics Basis Chapter 4: Power and Particle Control, Nucl. Fusion **47** (2007) S203.

[42]   A. Kallenbach et al., "Partial detachment of high power discharges in ASDEX Upgrade", paper presented at 25th IAEA Int. Conf. on Fusion Energy St. Petersburg (2014) EX/7-1.

[43]   A. Kallenbach et al., Nucl. Fusion **52** (2012) 122003.

[44]   F. Reimold et al., submitted to Nucl. Fusion (2014).

[45]   S. Potzel et al., Nucl. Fusion **54** (2014) 013001.

[46]   L. Aho-Mantila, paper presented at 25th IAEA Int. Conf. on Fusion Energy St. Petersburg (2014) TH/3-3.

[47]   F. Reimold, et al., 21st PSI conference, submitted to Journal Nucl. Materials (2014).

[48]   C. Giroud et al., Nucl. Fusion **53** (2013) 113025.

[49]   J. Schweinzer et al., paper presented at 25th IAEA Int. Conf. on Fusion Energy St. Petersburg (2014) EX/9-4.

[50]   J. Schweinzer et al., Nucl. Fusion **51** (2011) 113003.

[51]   H. Zohm et al., Fus. Eng. Design **88** (2013) 428.

[52]   A. Bock et al., "Confinement and stability of plasmas with externally driven steady-state elevated q-profiles", to be presented at the DPG Spring Meeting, Bochum, http://www.dpg-verhandlungen.de/year/2015/conference/bochum/static/p22.pdf (2015).

Appendix: The ASDEX Upgrade Team

J. Ahn[1], L. Aho-Mantila[2], S. Äkäslompolo[3], C. Angioni, O. Asunta[3], M. de Baar[4], M. Balden, L. Barrera Orte, K. Behler, J. Belapure, A. Bergmann, J. Bernardo[5], M. Bernert, M. Beurskens[6], A. Biancalani, R. Bilato, G. Birkenmeier, V. Bobkov, A. Bock, A. Bogomolov[4], T. Bolzonella[7], J. Boom, B. Böswirth, C. Bottereau[1], A. Bottino, H. van den Brand[4], F. Braun, S. Brezinsek[8], F. Brochard[9], A. Buhler, A. Burckhart, Y. Camenen[1], P. Carvalho[5], G. Carrasco[6], C. Cazzaniga[7], D. Carralero, L. Casali, M. Cavedon, C. Challis[6], A. Chankin, I. Chapman[6], F. Clairet[1], I. Classen[4], S. Coda[10], R. Coelho[5], J.W. Coenen[8], L. Colas[1], G. Conway, S. Costea[11], D.P. Coster, G. Croci[12], G. Cseh[13], A. Czarnecka[14], C. Day[15], P. de Marné, P. Denner[8], R. D'Inca, D. Douai[1], R. Drube, M. Dunne, B.P. Duval[10], R. Dux, T. Eich, S. Elgeti, K. Engelhardt, K. Ertl, B. Esposito[7], E. Fable, U. Fantz, H. Faugel, F. Felici[16], S. Fietz, A. Figueredo[5], R. Fischer, O. Ford, P. Franzen, L. Frassinetti[17], M. Fröschle, G. Fuchert[18], H. Fünfgelder, J.C. Fuchs, K. Gál, S. Garavaglia[12], M. Garcia-Muñoz[19], B. Geiger, L. Giannone, E. Giovannozzi[7], C. Gleason-González[15], T. Görler, T. Goodman[10], G. Gorini[12], S. da Graca[5], A. Gräter, G. Granucci[12], H. Greuner, J. Grießhammer, M. Groth[3], A. Gude, S. Günter, L. Guimarais[5], G. Haas, A.H. Hakola[2], T. Happel, J. Harrison[6], D. Hatch, V. Hauer[15], T. Hauff, B. Heinemann, S. Heinzel, T. Hellsten[17], P. Hennequin[20], A. Herrmann, E. Heyn[21], J. Hobirk, M. Hölzl, T. Höschen, J.H. Holm[22], C. Hopf, F. Hoppe, L. Horvath[23], A. Houben, A. Huber[8] , V. Igochine, T. Ilkei[11], W. Jacob, A.S. Jacobsen[22], J. Jacquot, M. Janzer, F. Jaulmes[4], F. Jenko, T. Jensen[22], E. Joffrin[1], C. Käsemann, A. Kallenbach, S. Kálvin[13], M. Kantor[4], A. Kappatou[4], O. Kardaun, J. Karhunen[3], D. Kim[10], S. Kimmig, A. Kirk[6], H.-J. Klingshirn, M. Kocan, F. Koch, G. Kocsis[13], A. Köhn[18], M. Köppen, J. Kötterl, R. Koslowski[8], M. Koubiti[1], M. Kraus, K. Krieger, A. Krivska[24], D. Kogut[1], A. Krämer-Flecken[8], T. Kurki-Suonio[3], B. Kurzan, K. Lackner, F. Laggner[25], P.T. Lang, P. Lauber, N. Lazányi[23], A. Lazaros[26], A. Lebschy, F. Leuterer, Y. Liang[8], Ch. Linsmeier, B. Lipschultz[27], A. Litnovski[8], A. Lohs, N.C. Luhmann[28], T. Lunt, A. Lyssoivan[6], J. Madsen[22], H. Maier, O. Maj, J. Mailloux[6], E. Maljaars[16], A. Mancini[12], A. Manhard, K. Mank, M.-E. Manso[5], P. Mantica[12], M. Mantsinen[29], P. Manz, M. Maraschek, E. Markina, C. Martens, P. Martin[30], A. Mayer, M. Mayer, D. Mazon[1], P.J. McCarthy[31], R. McDermott, G. Meisl, H. Meister, A. Medvedeva, P. Merkel, R. Merkel,

V. Mertens, H. Meyer[6], O. Meyer[1], D. Milanesio[7], J. Miettunen[3], A. Mlynek, F. Monaco, A. Moro[12], D. Moseev, H.W. Müller, S. Müller[32], M. Münich, F. Nabais[5], A. Nemes-Czopf[13], G. Neu, R. Neu, A.H. Nielsen[22], V. Nikolaeva[5], S.K. Nielsen[22], M. Nocente[12], B. Nold[18], J.-M. Noterdaeme, S. Nowak[12], M. Oberkofler, R. Ochoukov, T. Odstrcil, G. Papp, H.K. Park[33], A. Pau[7], G. Pautasso, F. Penzel, P. Petersson[17], P. Piovesan[30], C. Piron[30], B. Plaum[18], B. Plöckl, V. Plyusnin[5], Y. Podoba, G. Pokol[23], F. Pompon, E. Poli, K. Polozhiy, L. Porte[10], S. Potzel, R. Preuss, D. Prisiazhniuk, T. Pütterich, M. Ramish[18], C. Rapson, J. Rasmussen[22], S.K. Rathgeber, G. Raupp, D. Réfy[13], M. Reich, F. Reimold, M. Reinke[27], T. Ribeiro, R. Riedl, D. Rittich, G. Rocchi[12], M. Rodriguez-Ramos[19], V. Rohde, J. Roth, M. Rott, M. Rubel[17], F. Ryter, S. Saarelma[6], M. Salewski[22], A. Salmi[2], L. Sanchis-Sanchez[19], G. Santos[5], J. Santos[5], O. Sauter[10], A. Scarabosio, G. Schall, K. Schmid, O. Schmitz[32], P.A. Schneider, W. Schneider, M. Schneller, R. Schrittwieser[11], M. Schubert, T. Schwarz-Selinger, J. Schweinzer, B. Scott, T. Sehmer, M. Sertoli, A. Shalpegin[9], G. Sias[7], M. Siccinio, B. Sieglin, A. Sigalov, A. Silva[5], C. Silva[5], P. Simon, J. Simpson[6], A. Snicker[3], F. Sommer, C. Sozzi[12], M. Spolaore[7], M. Stejner[22], J. Stober, F. Stobbe, U. Stroth, E. Strumberger, K. Sugiyama, H.-J. Sun, W. Suttrop, T. Szepesi[13], B. Tál[13], T. Tala[2], G. Tardini, C. Tichmann, D. Told, L. Tophøj[22], O. Tudisco[7], U. von Toussaint, G. Trevisan[30], W. Treutterer, M. Tripský[24], M. Valisa[12], M. Valovic[6], P. Varela[5], S. Varoutis[15], D. Vezinet, N. Vianello[30], J. Vicente[5], T. Vierle, E. Viezzer, C. Vorpahl, D. Wagner, X. Wang, T. Wauters[24], I. Weidl, M. Weiland, A. Weller, R. Wenninger, B. Wieland, M. Wiesinger[25], M. Willensdorfer, B. Wiringer, M. Wischmeier, R. Wolf, E. Wolfrum, D. Wünderlich, E. Würsching, Z. Yang, Q. Yu, I. Zammuto, D. Zarzoso, D. Zasche, M. van Zeeland[34], T. Zehetbauer, M. Zilker, S. Zoletnik[13], H. Zohm.

IPP, Garching, Germany;

[1]CEA, IRFM, Cadarache, France;

[2]VTT, Espoo, Finland;

[3]Tekes, Aalto University, Helsinki, Finland;

[4]FOM-Institute DIFFER, TEC, Nieuwegein, The Netherlands;

[5]Instituto de Plasmas e Fusão Nuclear, IST, Lisbon, Portugal;

[6]CCFE Fusion Association, Culham Science Centre, UK;

[7]C.R.E, ENEA Frascati (Rome), Italy;

[8]Forschungszentrum Jülich, Germany;

[9]Institut Jean Lamour, CNRS, University of Nancy, France;

[10]CRPP-EPFL, Lausanne, Switzerland;

[11]ÖAW, University of Innsbruck, Austria;

[12]ENEA, IFP, CNR, Milano, Italy;

[13]Wigner Research Centre for Physics, Budapest, Hungary;

[14]Warsaw University of Technology, Warsaw, Poland;

[15]KIT, Eggenstein-Leopoldshafen, Germany;

[16]Technische Universiteit Eindhoven, The Netherlands;

[17]VR, Stockholm, Sweden;

[18]IGVPT, Universität Stuttgart, Germany;

[19]FAMN Department, Faculty of Physics, University of Seville, Seville, Spain;

[20]LPP, CNRS, Ecole Polytechnique, Palaiseau, France;

[21]Institut für Theoretische Physik - Computational Physics, TU, Graz, Austria;

[22]DTU, Kgs. Lyngby, Denmark;

[23]Budapest University of Technology and Economics, Budapest, Hungary;

[24]ERM/KMS, Brussels, Belgium;

[25]ÖAW, IAP, TU Wien, Austria;

[26]Hellenic Republic, Athen, Greece;

[27] University of York, York Plasma Institute, UK;

[28]University of California, Davis, CA, USA;

[29]ICREA-BSC, Barcelona, Spain;

[30]Consorzio RFX, ENEA, Padova, Italy;

[31]DCU, University College, Cork, Ireland;

[32]University of California, San Diego, CA, USA;

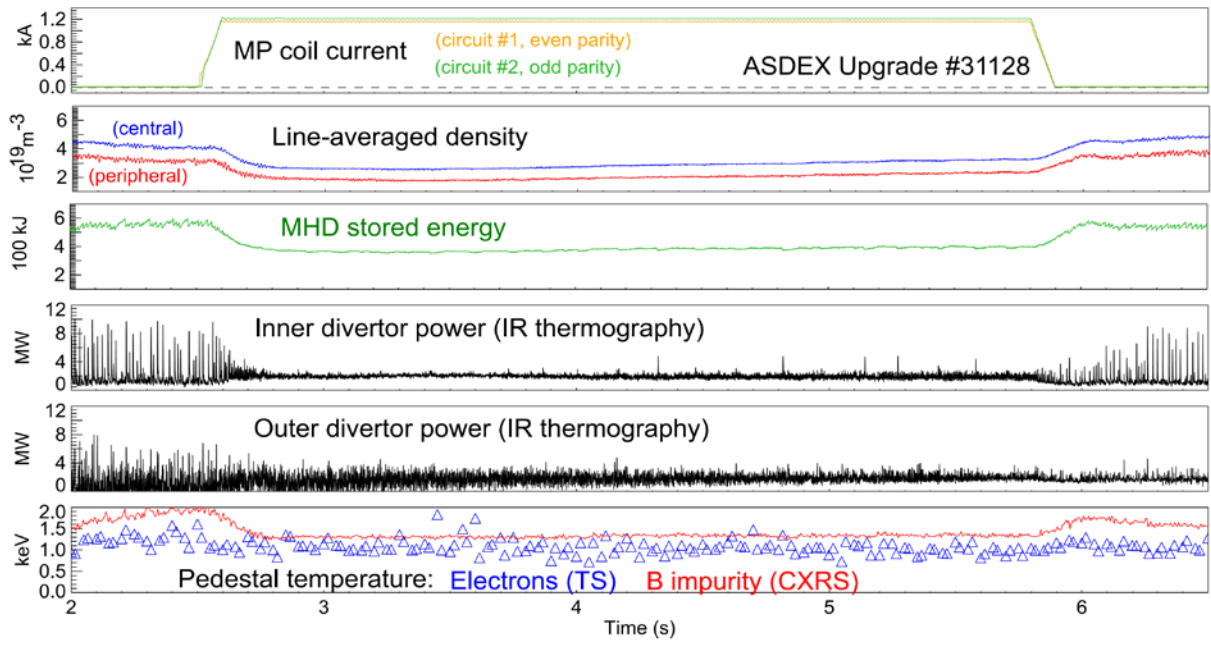[33]Gwacheon, South Korea;

[34]General Atomics, San Diego, CA, USA.

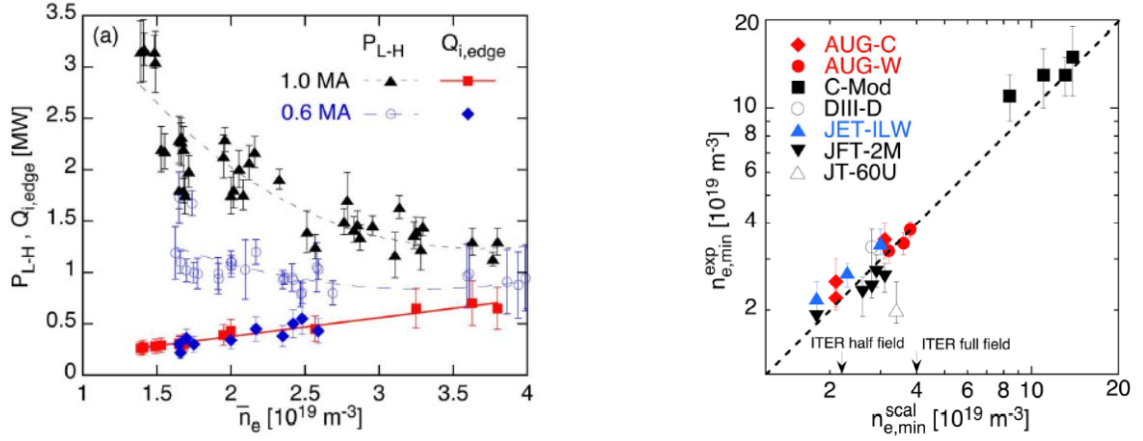FIG.1: ELM suppression with n=2 RMPs at low collisionality in ASDEX Upgrade.

FIG.2: Left: density dependence of the global threshold P_{LH} and the edge ion heat flux $Q_{i.edge}$ at the L-H transition. The ion heat flux unifies all measurements and smoothly connects to the intermediate branch where the linear density scaling is valid for P_{LH}, too. Right: a scaling for the density at which P_{LH} has its minimum based on electron-ion heat exchange unifies the points from the ITPA database.
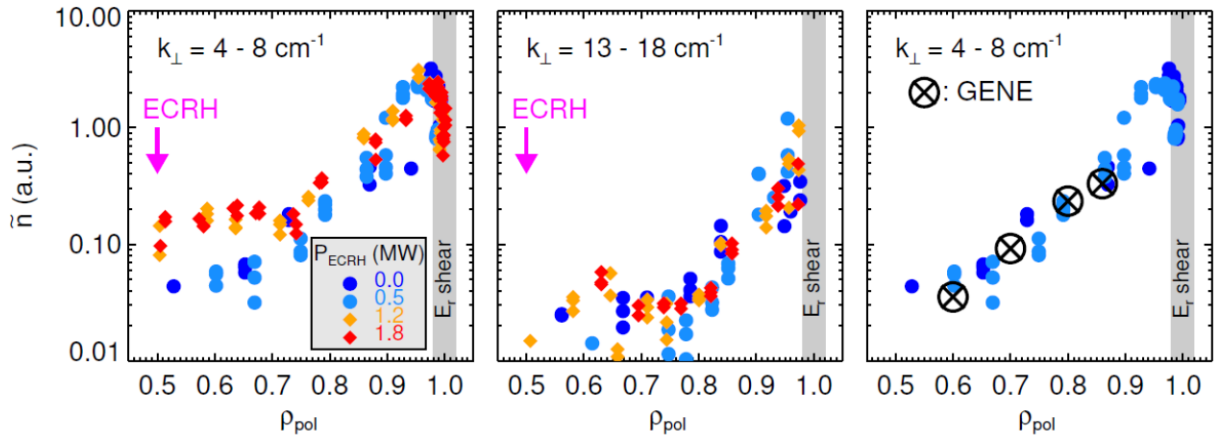
FIG.3: radial profiles of the RMS value of density fluctuation amplitude during an ECRH power scan at half radius in H-mode. While the large scale turbulence level (left) increases, the small scale level (middle) does not. GENE (right) reproduces quantitatively the radial variation of the turbulence level.
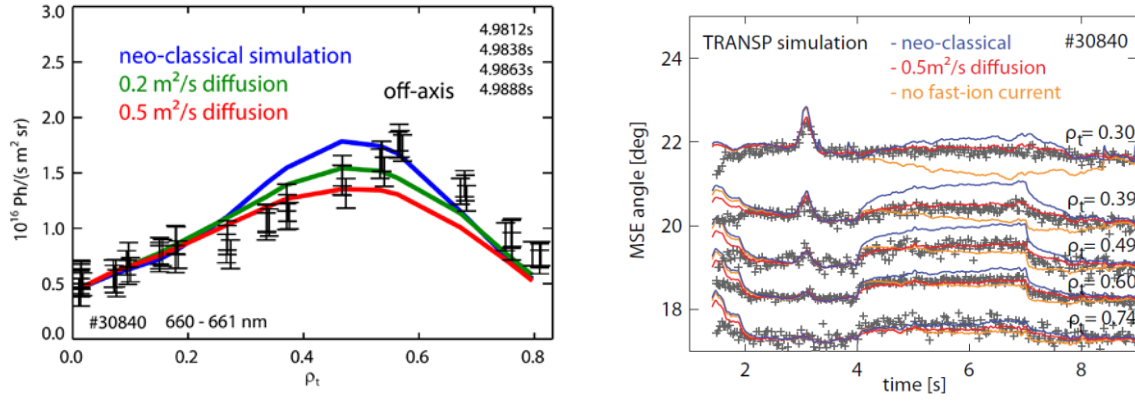
FIG.4: Analysis of fast ion behaviour during off-axis NBCD. Left: in high power cases, the measured FIDA emission profiles (black data points from different time points in a stationary phase) are inconsistent with neo-classical slowing down (blue line) in the region of interest for NBCD, i.e. between ρ=0.3 and ρ=0.5. Assuming an anomalous component of fast ion transport (green and red lines) gives a better match. Right: the temporal evolution of MSE channels during off-axis NBI (4 - 7 s) also indicates anomalous diffusion of fast ions in this case.
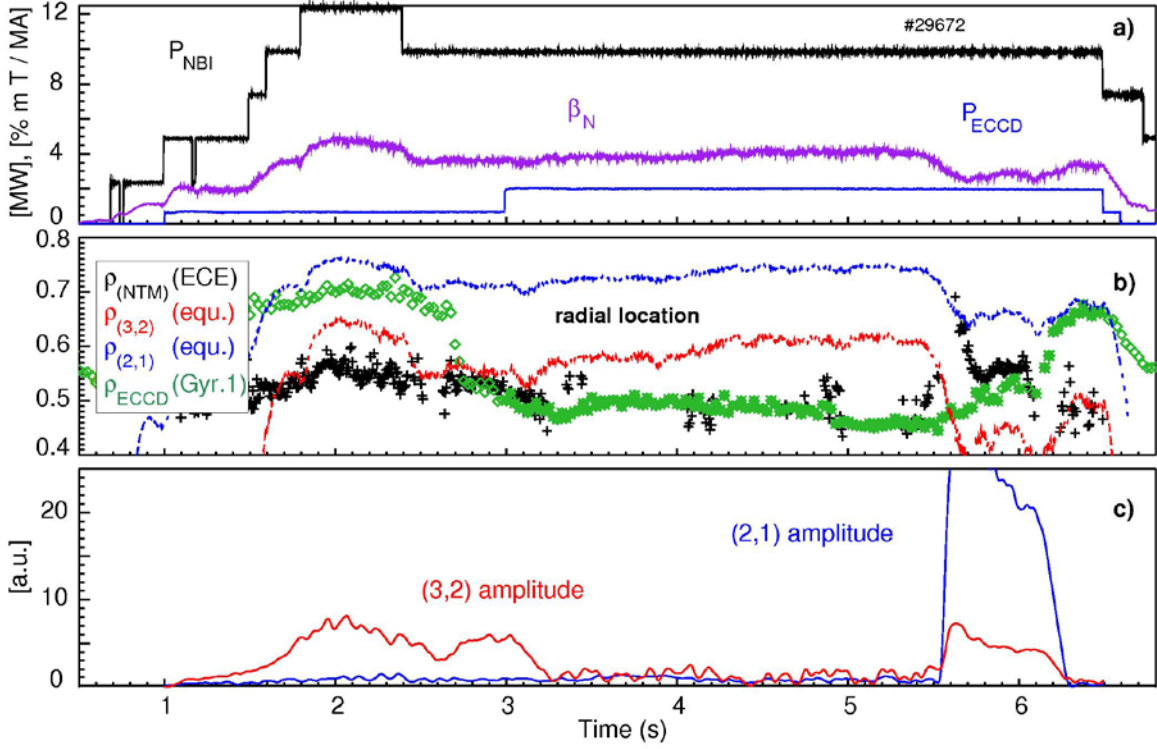
FIG.5: Feedback controlled NTM stabilization with variable target: the discharge control system (DCS) initially targets and suppresses a (3,2) NTM until a (2,1) NTM occurs and is recognized by the DCS from comparing the mode amplitudes shown in panel c). Then, deposition is shifted from the q=1.5 to the q=2 surface and the (2,1) NTM is suppressed. Panel b) shows the location of the resonant surfaces deduced form equilibrium reconstruction labeled $\rho_{(m,n)}$(equ.), the location of the NTM as targeted by the control system deduced from ECE, labeled ρ_{NTM}(ECE), and the deposition location of the gyrotron operated in feedback labeled ρ_{ECCD}. For the latter, open symbols mean that the gyrotron is off while asterisk means the gyrotron power is on.
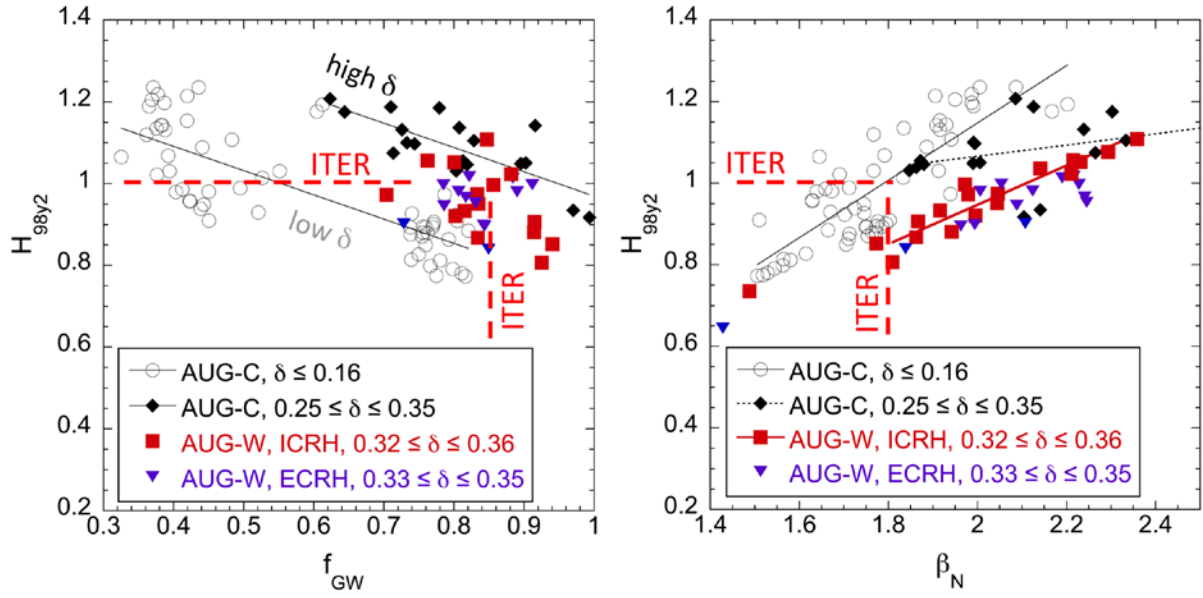
FIG.6: Database of $q_{95} = 3$ H-mode discharges in ASDEX Upgrade with C-wall (black points) and W-wall (red and blue points). The left part shows that similar to results obtained with the C-wall, increasing good confinement can be reached at high density if the triangularity is high enough. However, as seen in the right part these points lie at higher β_N in the existence diagram, which is connected to the operational constraints from the W-wall (mainly the need for higher gas puff).
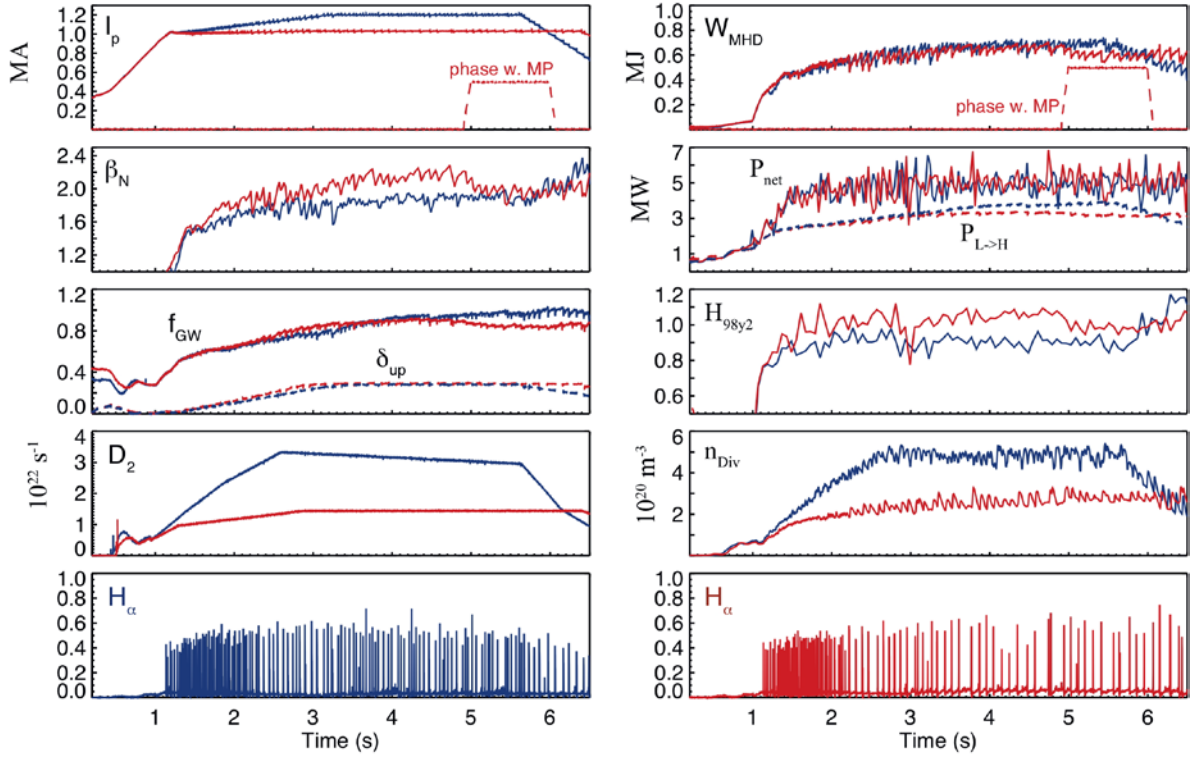
FIG.7: ITER Q=10 scenario with baseline ($q_{95} = 3$, #31146, blue) and reduced current ($q_{95} = 3.6$, #31148, red). Due to the increase in β_N and H, the case with reduced current has the same stored energy, i.e. would have the same fusion power as long as the temperature is close to the optimum value for D-T fusion.
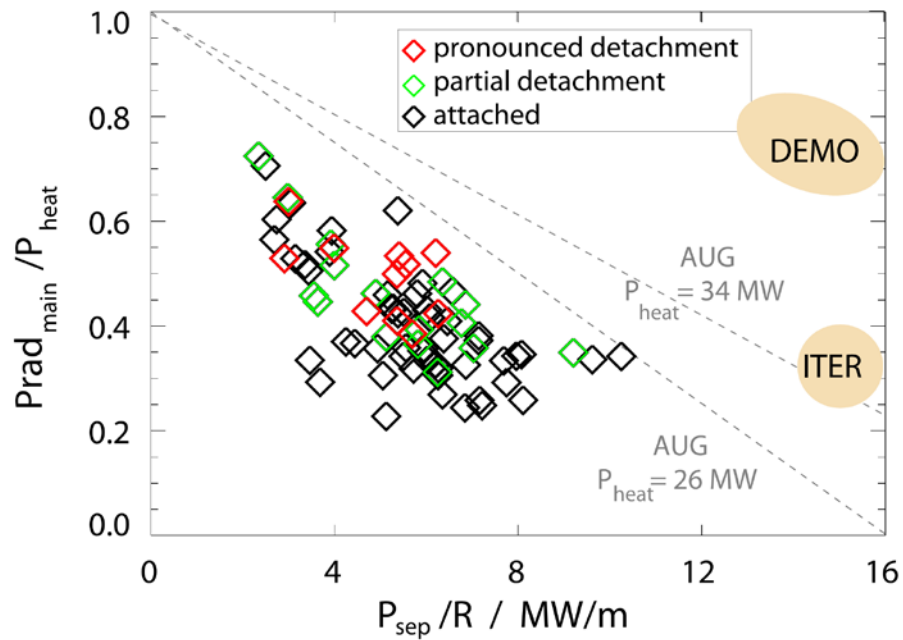
FIG.8: operational space of ASDEX Upgrade exhaust scenario studies in terms of P_{sep}/R versus core radiated fraction (the main chamber radiation is taken as proxy for the core radiation, i.e. SOL radiation in the main chamber is included for diagnostics resolution reasons. Also shown are the operational points envisaged for ITER and DEMO. For the envisaged upgrade to simultaneous injection of 34 MW, the ITER value of P_{sep}/R can be accessed.